# A Versatile IF Polarimeter at the IRAM 30m Telescope

C. Thum[a], H. Wiesemeyer[a], D. Morris[a], S. Navarro[b], and M. Torres[a]

[a] IRAM, Grenoble, France
[b] IRAM, Granada, Spain

## ABSTRACT

We report on the commissioning of a polarimeter operating at the intermediate frequency (150 MHz) of the IRAM 30m telescope. The polarimeter adds, with suitable phase shifts, the amplitudes of two orthogonally linearly polarized heterodyne receivers, and determines from these signals all four Stokes parameters. The polarimeter allows continuum as well as spectral line observations in all millimeter atmospheric windows accessible with the 30m telescope.

The instrumental phase between the two receivers, controlled through a phase shifter, does not exceed one degree (rms) at 3mm. Instrumental polarization on boresight is found to be small, below one percent for Stokes $U$ and $V$. Limitations due to beam polarization are discussed. We present results from the first large scale 3mm polarization survey started in 1999. About 100 Active Galactic Nuclei with flux densities stronger than 0.8 Jy were observed, many of them repeatedly. Linear polarization larger than 10 percent is found in several sources at several epochs.

We briefly describe results from two spectro–polarimetric surveys: SiO maser stars and methanol masers. Polarization is easily detected in both groups.

**Keywords:** IF Polarimeter, Millimeter Astronomy, AGN, Moon

## 1. INTRODUCTION

A polarimeter operating at the intermediate frequency (IF) of a radiotelescope uses the well known concept of the correlation receiver.[1,2] The advantages of the IF polarimeter over alternatives employing switching waveplates consist in a higher observing efficiency, frequency agility, and the capability to measure all four Stokes parameters simultaneously. Furthermore, any elements moving in the beam which are prone to generate instabilities of the spectroscopic baseline are avoided. On the down side, two (orthogonally polarized) rather than just one receivers are needed whose relative phase needs to be controlled carefully.

Spectropolarimetric observations at single dish radio telescopes have so far nearly always used waveplates.[3–5] The only exception was reported recently from Arecibo where a correlation technique used.[6] With the installation of dual polarization receivers at the IRAM 30m telescope in 1999, we started the commissioning of a prototype IF polarimeter described here.

## 2. BASIC PRINCIPLES

The design of the IF polarimeter (Fig. 1) is centered on two power splitters, one of them shifting one of its two output channels by 90°. The four outputs are fed to two hybrid junctions which form the sum and difference of the incoming waves. Globally, the polarimeter generates from two input waves, A and B, four output waves whose amplitudes are the sum of the two input waves, but whose relative phase is shifted by 0, 90, 180, and 270 degrees. The characteristics of the splitters and junctions used limit our device to a narrow band of about 40 MHz centered at 150 MHz.

Further author information: (Send correspondence to C.T.)
C.T.: E-mail: thum@iram.fr, Tel.: +33-476-824839
E-mail of coauthors: wiesemey@iram.fr, navarro@iram.es, morris@iram.fr, torres@iram.fr

Connecting the inputs A and B to two orthogonally linearly polarized receivers converts the device into an IF polarimeter. We consider the two plane waves propagating in the $z$–direction towards the polarimeter:

$$e_H(z,t) = E_H \sin(\omega t - kz) \tag{1}$$
$$e_V(z,t) = E_V \sin(\omega t - kz + \delta) \tag{2}$$

The relative phase $\delta$ together with the relative amplitude of the horizontal and vertical electric fields, $E_V$ and $E_H$, contain the polarization characteristics of the incident radiation field. The polarimeter adds different phase lags *theta* to these waves as listed in Tab. 1. The power of the output waves

$$< |e_H + e_V|^2 > = < (e_H + e_V)(e_H + e_V)^* > \quad = \quad < E_H^2 > + < E_V^2 > + \, 2 \, < E_H E_V \cos\theta >$$

consists of the sum of the power of the two input waves and a correlation term. Tab. 1 shows that the value of the correlation term is different for the 4 output signals $S_1$ to $S_4$. The Stokes parameters $I, U,$ and $V$ can be derived from these signals (Tab. 2). Stokes $Q$, the power difference between the two incoming waves, cannot be obtained in this way and is measured as described below (sect. 3).

**Table 1.** IF polarimeter. Phase offsets $\theta_A$ and $\theta_B$, and the resulting correlation term.

| output channel | descriptive designation | phase lags $\theta_A$ | $\theta_B$ | total | correlation term $\cos\theta$ |
|---|---|---|---|---|---|
| $S_1$ | $A + B$ | 0 | 0 | $\delta$ | $\cos\delta$ |
| $S_2$ | $A - B$ | 0 | 180 | $\delta + 180$ | $-\cos\delta$ |
| $S_3$ | $A^* + B$ | 90 | 0 | $\delta + 90$ | $\sin\delta$ |
| $S_4$ | $A^* - B$ | 90 | 180 | $\delta + 270$ | $-\sin\delta$ |

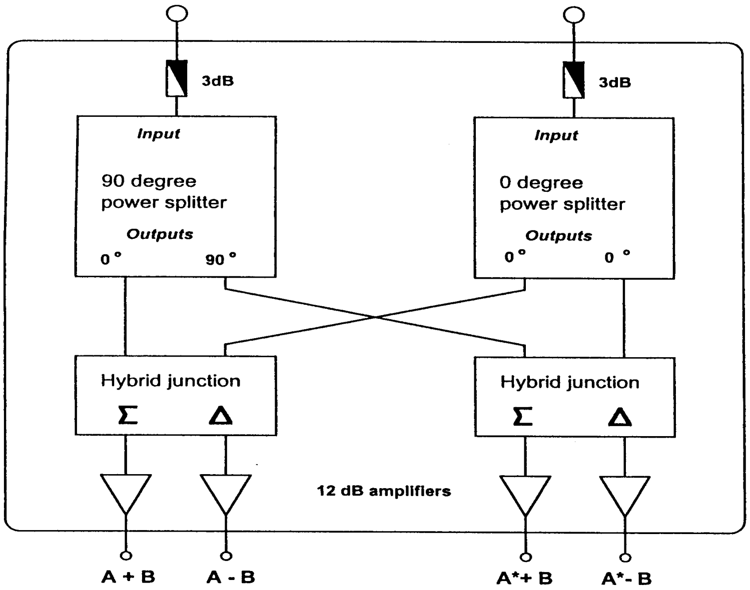


**Figure 1.**
Schematic diagram of the IF polarimeter. Hybrid junctions form the sum (Σ) and difference (Δ) of the two input signal amplitudes, once with an additional phase shift of 90° (starred output channels) and once without. Note the presence of amplifiers and attentuators which affect the gain of these 4 signals with respect to signals bypassing the polarimeter. The length of all connecting cables is carefully matched.

## 3. IMPLEMENTATION

The beam from the telescope is separated in the Nasmyth receiver cabin by a wire grid into horizontal and vertical linearly polarized radiation which is mixed with local oscillators in two SIS mixers housed in separate

**Table 2.** The Stokes parameters derived from the 6 spectrometer output signals.

| | |
|---|---|
| $I = \frac{1}{2}(S_1 + S_2) = \frac{1}{2}(S_3 + S_4)$<br>$U = \frac{1}{2}(S_1 - S_2)$<br>$V = \frac{1}{2}(S_3 - S_4)$ | using the polarimeter |
| $I = S_5 + S_6$<br>$Q = S_5 - S_6$ | bypassing the polarimeter |

dewars (Fig. 2). The IF signals are further downconverted to the observatory's standard IF $(342 \pm 256)$ MHz. The polarimeter is installed immediately following the downconverters. Its four output signals ($S_1$ to $S_4$) are connected to 4 identical sections of the autocorrelator in the backend room. Two additional cables connect the receivers directly to correlator sections $S_5$ (A100) and $S_6$ (B100) permitting measurements of Stokes Q spectra (Tab. 2). The location of the polarimeter in the receiver cabin makes observations insensitive to phase changes in the more than 100m long IF cables.

The Stokes parameters used in this contribution refer to a right–handed coordinate system $(x, y)$ at rest in the Nasmyth receiver cabin where the horizontal axis $x$ points towards increasing azimuth, and $y$ points upwards.

Departing from the routine non–polarimetric setup, the two local oscillators are referenced to a common synthesizer. The same modification turned out to be necessary for the two downconverters running at 1.5 GHz. These modifications assure that the two receivers have a constant relative phase which can be set to zero with the computer controlled phase shifter inserted in the path to one of the downconverters (Fig. 2).

## 4. CALIBRATION

### 4.1. Delay and Phase

The correct operation of the polarimeter demands that the paths of the H and V waves between the telescope aperture plane and the polarimeter input are equal. We check the most critical fraction of these paths with the help of a signal generator operated at 86 GHz and installed before the grid splitting the paths to the two receivers. The generated linearly polarized signal was oriented at 45° with respect to the receivers. The variation across the nominal bandwidth of the relative phase of the two resulting sine waves was minimized by introducing pieces of cable into the path of one receiver.

The signal generator was also used for measurements of the phase between the receivers. A phase meter* which was installed before the polarimeter (Fig. 2) multiplies the IF power of these coherent monochromatic signals and generates a DC output voltage related to the phase difference. The voltage calibrated in degrees of phase difference was used to reset the phase difference to zero with the help of the phase shifter (Fig. 2). This measurement which takes less than 3 min could be made as often as needed during polarimetric observations (see sect. 5.1).

### 4.2. Polarity of Stokes Parameters

Stokes parameters $Q, U,$ and $V$ are derived from differences between the recorded spectra $S_1$ to $S_4$ (Tab. 2) and may therefore be positive or negative. The correct sign for Stokes $Q$ (horizontal $-$ vertical) is unambiguous, but the polarities of $U$ and $V$ need calibration.

The polarity of $U$ is readily determined by an observation of a celestial linear polarization calibrator. The Crab Nebula is the best such source, as is flux density and polarization at 3mm are strong, and the source does

*The unit consists of a mixer whose DC output voltage is maximum if the two incident waves, amplified and strongly filtered, are in phase.

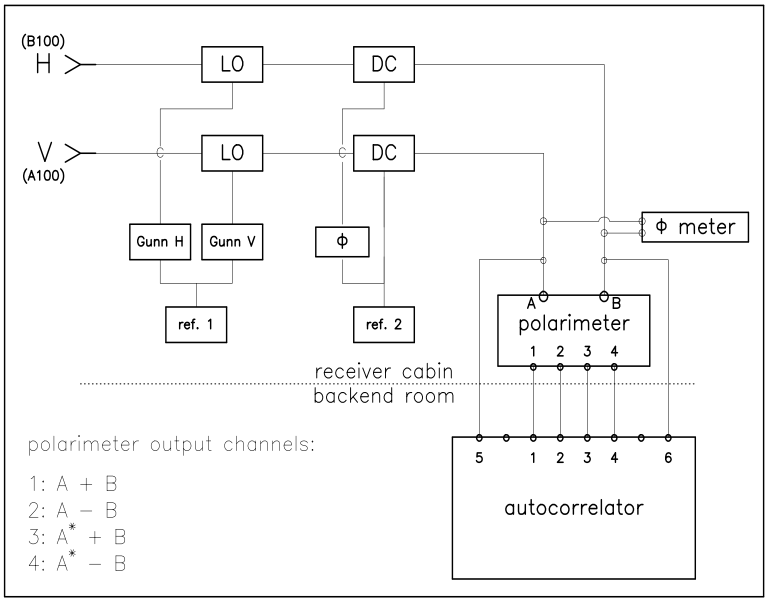


**Figure 2.** Implementation of the IF polarimeter in the Nasmyth receiver cabin of the IRAM 30m telescope. The signals from the horizontally (H) and vertically (V) polarized receivers are mixed with local oscillators (LO) referenced to a common synthesizer (ref. 1). The signals are further downconverted (DC) to an intermediate frequency of 150 MHz, before they are connected to the polarimeter. A phase shifter ($\Phi$) and a phase meter ($\Phi$ meter) are also included. Signals are detected in the autocorrelator whose 6 sections are connected to the receiver cabin by the standard 4 IF cables from the IF distribution box (not shown) and two additional cables (no. 5 and 6).

not vary. A high frequency map of its linear polarization[7] shows that the polarization vector does not vary much across the nebula.

The polarity of $V$ was measured by inserting a quarter–wave plate optimized for 86 GHz into the beam before the beam separator grid. Aligning the quarter–wave plate axis by $\pm 45°$ with respect to the signal generator tuned to the same frequency converted its linearly polarized beam into well defined left or right hand circular polarization.

## 4.3. Polarimeter gain

The hot/cold/sky calibration corrects for atmospheric and spillover losses and provides the conversion factor from backend counts to antenna temperature for signals $S_5$ and $S_6$ in the usual way, as these signals bypass the polarimeter. Signals $S_1 \ldots S_4$, however, represent weighted sums of signals from two receivers, and these signals have additional gains due to their passage through the polarimeter. These additional complex gains must be taken into account in a homogenous calibration scale for all signals $S_1 \ldots S_6$.

There are 8 such additional gain factors, $g_{ij}$, which represent the differential gain picked up along the paths through the polarimeter from input port $i = 1, 2$ (A and B in Fig. 2) to output port $j = 1 \ldots 4$. We determined these 8 gains in two ways, *(i)* with the network analyzer in the Grenoble receiver laboratory and *(ii)* with the signal generator at the telescope. Results from the network analyzer were obtained over the full frequency range relevant for the polarimeter. Over the 40 MHz band, centered on 175 MHz, the maximum gain imbalance is $\lesssim 0.01$ dB and the differential phase error $\lesssim 0.5°$. A full description of these results appears elsewhere.

At the telescope, we measure the differential gains and the phase steps of the polarimeter directly, using the signal generator at 150 MHz, near the center of nominal polarimeter bandpass. We detected the quasi–monochromatic power from the signal generator with the autocorrelator backend, while the relative phase between the receivers was varied over 360° with the phase shifter. The detected power, after integration of the

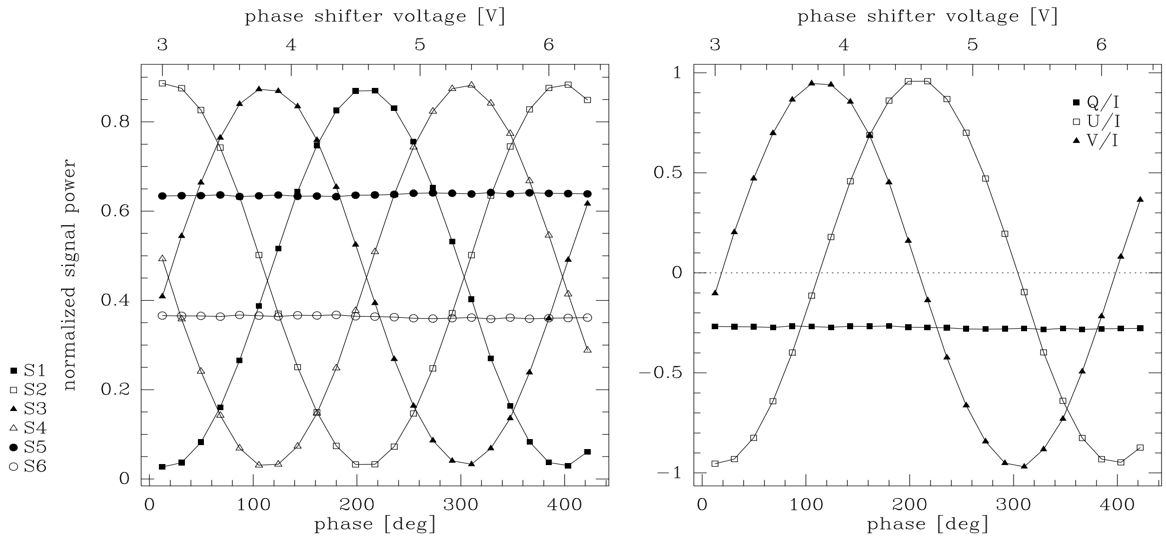


**Figure 3.** Response to the signal generator (linearly polarized at 45°) as a function of the instrumental phase. The 6 signals recorded by the autocorrelator backend (Tab. 2) are normalized by the total power and sine waves are fitted (left frame). Normalized Stokes parameters are derived and corrected for the polarimeter gains as derived from the sine waves (right frame). The true instrumental phase is near 200°, where the signal appears fully linearly polarized ($V = 0$).

instrumentally broadend line profile and normalization with the total power, $I = S_5 + S_6$, is shown in Fig. 3 (upper left frame). The normalized signals $S_5/I$ and $S_6/I$ which are not affected by the relative receiver phase are constant, whereas $S_1/I \ldots S_4/I$ vary in a nearly sinusoidal way as expected.

From a formal fit of sine waves to the normalized signals 1...6 (see appendix A) we derive *(i)* the 8 differential gains $g_{ij}$, *(ii)* the phase difference between the 4 sine waves, and *(iii)* the amplitude ratio of the electric fields of the signal generator in the two IFs. These results are listed in Tab. 3.

**Table 3.** Differential gains of the 8 paths through the polarimeter, from input ports A and B to output ports $i = 1 \ldots 4$. Results are derived from the fit of 4 sine waves (Fig. 3).

| | | | | |
|---|---|---|---|---|
| gains$(A,i)$ | 0.696 | 0.686 | 0.669 | 0.691 |
| gains$(B,i)$ | 1.264 | 1.302 | 1.314 | 1.280 |
| zero phase | $15.4 \pm 0.4 (1\sigma)$ | | | |
| amplitude ratio | $0.567 \pm 0.02$ | | | |

The differential gains are close to unity as expected with departures up to a maximum of $\sim 30\%$. The large zero phase is not relevant, as it will be set to zero in the manual phase calibration. The scatter of the zero phase, however, is an important charcteristic of the polarimeter. It shows that the 4 sine wave are correctly spaced out by 90° steps, with a peak–to–peak scatter smaller than 1°.

The amplitude ratio is found to be different from unity. This means that Stokes $Q \neq 0$, and the orientation of the signal generator is actually somewhat different from the 45° aimed for in the set up of the experiment. This difference was confirmed by later inspection of the signal generator mount.

The right panel of Fig. 3 shows the variation of the Stokes parameters $Q, U$, and $V$ with instrumental phase and the corresponding variation of the polarization degrees and of the polarization angle. The correct instrumental phase occurs at one of the zero crossings of Stokes $V$, where $p_C = 0$ and $p_L = 1$. In valid astronomical observations, this phase must be tracked as closely as possible.

## 5. PERFORMANCE

### 5.1. Phase stability

The performance of the IF polarimeter critically depends on how faithfully the phase $\delta$ of the radiation field (eqs. 1 and 2) is transported to the polarimeter. At this point, the phase difference between the two input signal is frozen, since only the *auto*correlations are measured from the polarimeter output signals.

Early in the commissioning of the polarimeter we noticed that the by far dominant source of phase variations originated in thermal drifts. Although the temperature in the receiver cabin is carefully controlled and, when the vertex is closed by a sailcloth window, does not vary by more than $\pm 1$ degree, we recorded quasi–periodic phase variations of up to $\pm 10°$, coarsely synchronized with the cabin temperature regulation cycle. These phase variations were easily reduced to about $\pm 1°$ by reducing the air flow in the cabin, better thermal insulation of the critical components including the phase meter, and other measures.

The main effect of a phase error is to transport power from Stokes $U$ to $V$. A false circular polarization signal is therefore obtained in the presence of strong linear polarization. The typical phase error of $\pm 1°$ would then cause a false $V/I = 1\%$ in the presence of $U/I \sim 50\%$, as may very occasionally be found, e.g. in SiO stars. For virtually all practical purposes, the phase stability reached in our setup is therefore sufficient.

### 5.2. Instrumental polarization

The next critical performance aspect concerns the sensitivity of the setup to effects which transport power from Stokes $I$ to the other Stokes parameters, commonly called instrumental polarization. We investigated these effects by frequently observing celestial sources with no or only weak polarization, like the planets and compact HII–regions. We show the results of a typical observing session as $Q, U$ and $V, U$ plots (Fig. 4). The weighted mean of these 86 GHz observations of 22 unpolarized continuum sources, HII regions and planets, gives the instrumental polarization, $Q_i, U_i$, and $V_i$, as indicated by dotted lines.

Only Stokes $Q_i$ is significantly different from zero. The observed small value can easily be explained by a systematic calibration difference between the two independently calibrated receivers which would go unnoticed in non–polarimetric spectroscopy. Such calibration errors do not affect $U_i$ and $V_i$ which are obtained from correlations between the two receivers.

The instrumental values, however, do not appear to be constant between observing sessions. These findings suggest that the instrumental polarizations found are not a characteristic of the polarimeter or the telescope. We suspect that they reflect small errors of the differential gains $g_{ij}$ (sect. 4.3). Such errors could come from inevitable variations of receiver gain. Receiver gain instabilities were measured to be of the order $\sim 3\,10^{-4}$ per sec, compatible with the observed magnitude of the $1\sigma$ errors of the instrumental polarization parameters which were obtained from measurements lasting a few minutes.

We regularly observe that the uncertainty in $Q_i$ is larger than in the other parameters. We attribute this effect to variations in the atmospheric emission which is more easily cancelled in the Stokes parameters derived from correlations.

### 5.3. Beam Polarization

Knowledge of the beam polarization is important when extended source are observed. Even for point sources, the beam polarization can introduce errors if pointing is not perfect. A few beam maps were made in the on–the–fly observing mode, using Venus and other planets. Beam maps in all 4 Stokes parameters are obtained simultaneously. All beam maps obtained are compatible with each other, and we show the results obtained from Venus (Fig. 5). The maps shown are convolved with the planet's disk of $16''$ size.

Whereas the deconvolved Stokes $I$ map gives a Gaussian beam of $27''$ half power width as expected at the observing frequency of 86 GHz, the other maps have weak and clearly bipolar patterns. In all maps obtained,

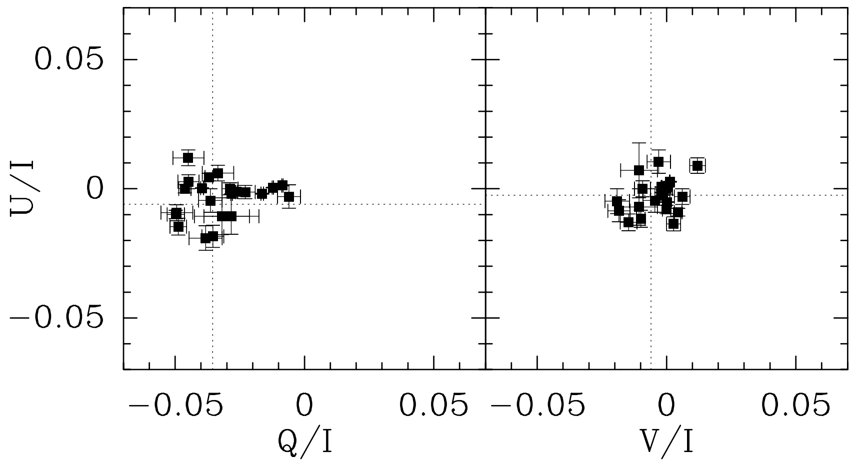


**Figure 4.** Instrumental polarization measured during the July 2001 session. Data obtained from 22 observations of unpolarized sources. The weighted means of the instrument Stokes parameters and the standard deviation are, in percent, $Q_i = -3.50 \pm 1.10, U_i = -0.60 \pm 0.80, V_i = -0.20 \pm 0.80$.

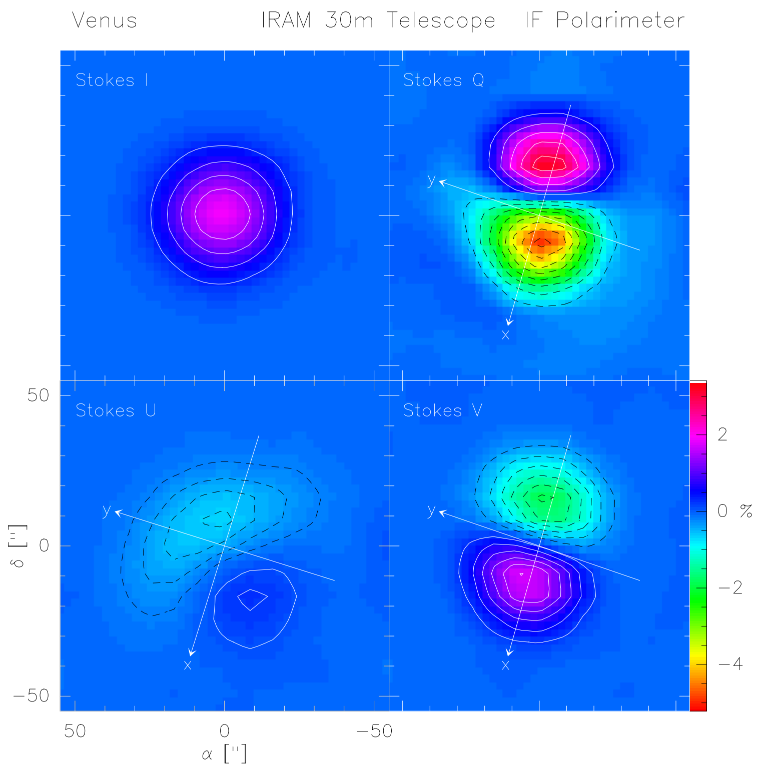


**Figure 5.** Beam maps of the Stokes parameters. The Stokes I beam (upperleft) is drawn with contours stepped by 20%. The other beam maps ($Q$: upper right, $U$: lower left, $V$: lower right) have a common grey scale indicated on the lower right frame. The contour lines, in percent, increase/decrease from ±0.6 in steps of 0.6% ($Q$), from ±0.15 in steps of 0.15 % ($U$), and from ±0.30 in steps of 0.30 ($V$). Negative contours are dashed. The $x, y$ coordinates indicate the horizontal/vertical direction at the polarization reference plane in the Nasmyth receiver cabin.

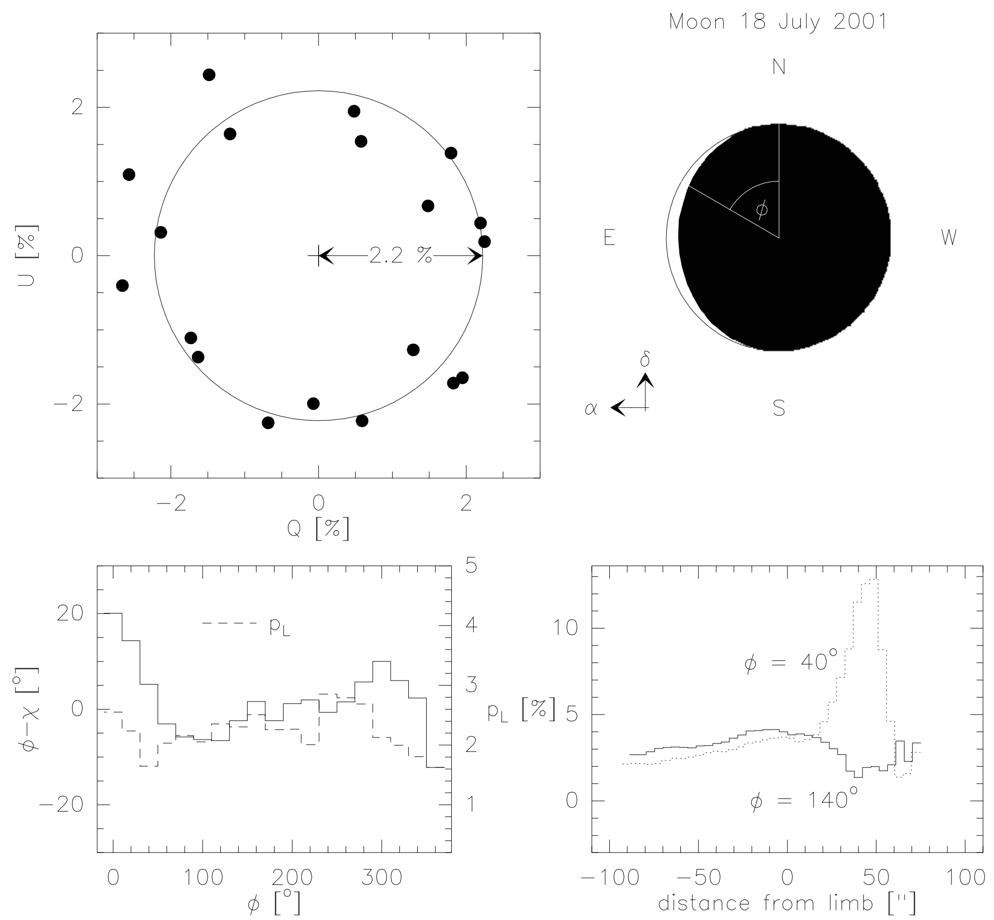


**Figure 6.** Polarization of the moon's limb observed at 86 GHz close to New Moon (upper right). The lower right frame shows two typical profiles of the linear polarization observed when scanning along a $220''$ long radial line centered on the limb (distance is positive outside the moon). Stokes $Q$ and $U$ at the innermost points of such scans, made in $20°$ steps along the moon's circumference, describe a circle centered on the origin (upper left). The polarization angle $\chi$ at these points follows closely their position angle $\phi$ (continuous line, lower right frame).

these patterns appear fixed in the Nasmyth coordinates $(x, y)$ of the polarization reference plane, although maps were taken at very different elevations. The $Q$ map is most easily interpreted as due to a slight misalignment between the receivers. A separation by $0.7''$, mostly along the Nasmyth horizontal, can explain the observed pattern. The Stokes $U$ and $V$ maps may point towards some misalignment in the telescope structure itself.

### 5.4. Polarization of the Moon's limb

As a further challenging check of the performance of the IF polarimeter we attempted to detect at 86 GHz the polarization of the moon's limb. Previous observations[8] at cm wavelengths report linear polarization of a few percent at positions near the limb. This weak polarization results mainly from Fresnel reflection on a smooth dielectirc sphere, but surface roughness and dielectirc inhomogeneities in the top layers of the lunar soil may also contribute. The 3mm polarization measurements may give information on the small scale properties of these effects.

We made 19 on–the –fly scans perpendicular to the moon's limb, spaced out 20° along its circumference. Each 220" long scan ($\sim$ 8 half power beam widths) was centered on the limb. At the time of observation (new moon) the temperature profile of the disk was nearly flat. Due to the strength of the total power signal

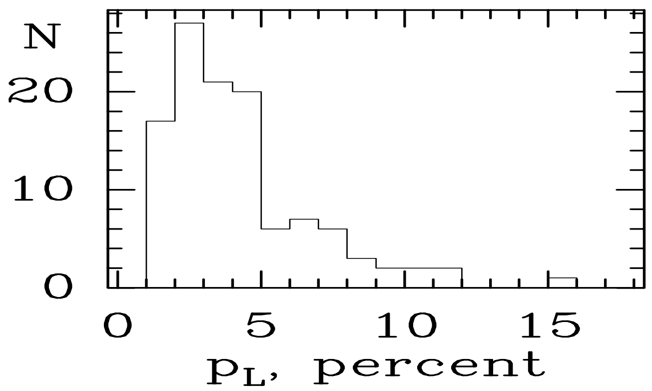


**Figure 7.** Histogram of the distribution of linear polarization, $p_L$, at 86 GHz of our AGN sample. Measurements are corrected for bias due to the positive definiteness of $p_L$.

the polarization response is strongly confused with instrumental effects. As the Stokes $U$ sidelobes are weak, the linear polarization response is dominated by the bipolar pattern of Stokes $Q$. Accordingly, this response depends on the orientation of the pattern with respect to the scanning direction. Fig. 6 (lower right frame) which shows two extreme profiles (corresponding to parallel and perpendicular orientation) clearly demonstrates this effect. On the inside of the limb the polarization signal weakens, but it does not reach zero at the end of the scans, about 4 beams (110") away from the limb. All scans, independent of the lunar position angle reach a very similar linear polarization degree of $p_L \sim 2.2\%$ (Fig. 6, upper left frame) which we take as the true polarization near the limb. The polarization angle never deviates more than 20° from the position angle of the scan indicating that the polarization is predominantly in the radial direction.

## 6. SOME ASTRONOMICAL RESULTS

Several regular polarimetry projects[9–11] have been scheduled already at the IRAM 30m telescope with the IF polarimeter. Here we show a few representative results.

### 6.1. Survey of Active Galactic Nuclei

During the commissioning period (November 1999 — July 2001) all pointing sources stronger than ca. 0.8 Jy at 86 GHz were observed in polarimetry mode. Although the narrow bandwidth of the IF polarimeter is clearly not optimum for continuum observations, linear polarization was detected in most of these sources which are all active galactic nuclei.[9] A total of 133 valid observations were made of 74 AGN of which 41 are QSO and 33 BL Lac objects. The sources where several observations were obtained often displayed variable linear polarization.

Fig. 7 shows the "snapshot" of the linear polarization distribution of this bright AGN population. The typical AGN appears linearly polarized at a $\sim 3\%$ level. But there is a tail of much stronger polarizations, up to 16%. Surprisingly few sources were found with very low linear polarization. These AGN observations greatly expand on previous work[12] and constitute the first 3mm polarization survey, complete down to $\gtrsim 1$ Jy and declination $> -20°$.

### 6.2. Spectropolarimetry

The two samples studied are both dominated by maser emission. Many of the SiO stars observed[10] were found to be strongly linearly polarized. Weak circular polarization was also present in a few stars. Fig. 8 shows the emission from the young massive star Orion IRc2 which originates in a bipolar outflow.[13] There are well defined spectral features with up to 40% linear polarization which may reflect magnetic fields embedded in the outflowing material and/or propagation effects of the maser.

Methanol masers, both class I and II, were surveyed[11] in several transitions at 3 and 2mm. The source M8 E (Fig. 9) is again a massive young star forming region where we detect strong linear, accompanied by little if any circular polarization. We expect our survey to characterize in a statistical sense the polarization properties of this maser which is virtually unexplored at millimeter wavelengths.

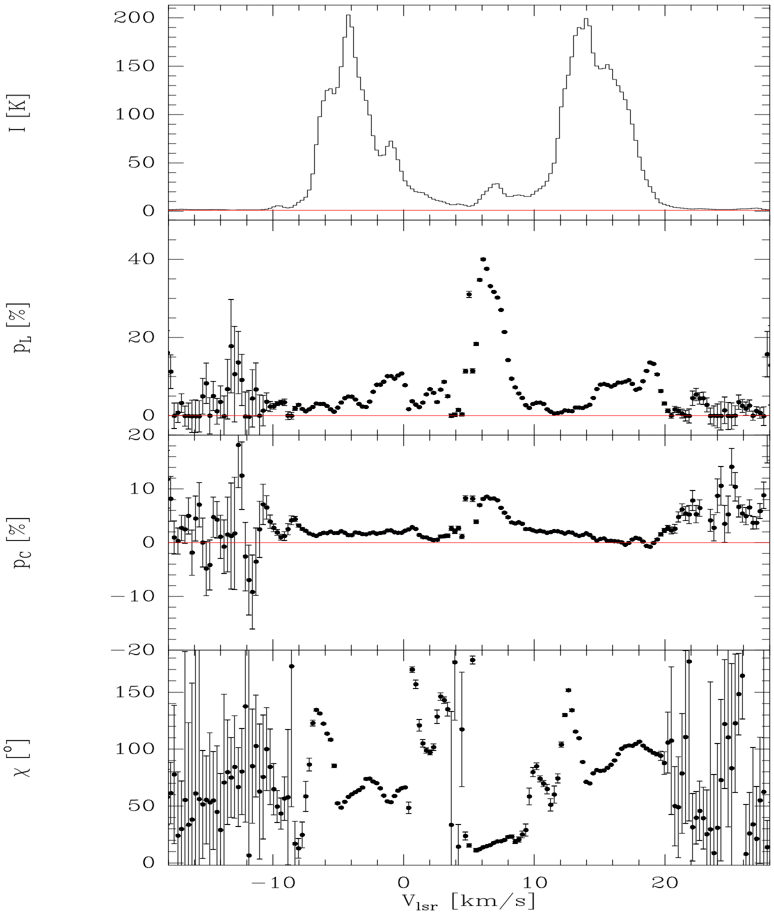


**Figure 8.**
Spectropolarimetric observation of the $v = 1, J : 2 \to 1$ transition of SiO in Orion IRc2.Stokes I is given in degrees of antenna temperature, $p_L$ and $p_C$ and fractional linear and circular polarization, and $\chi$ is the polarization angle, degrees, in the equatorial system.

## 7. CONCLUSION AND PLANS

We have demonstrated that the concept of an IF polarimeter works well in millimeter spectroscopy. The most serious limiting factors are currently the modest bandwidth (40 MHz) and the instrumental polarization (< 1 % in $U$ and $V$) resulting from gain drifts in the receivers. The somewhat large value in $Q$ (a few percent) is constant and can be precisely removed. The main source of instrumental phase variation has been identified as thermal drifts and effectively made negligible. The residual phase drifts are of the order of $\lesssim 1°$ rms. We found the beam to have weak polarized sidelobes which need more investigation.

The bandwidth constraint and the sensitvity to drifts will soon be reduced when we can make a fully digital cross correlation in the newly upgraded correlator backend VESPA. The IF polarimeter will then work in a way similar to an all digital interferometer.

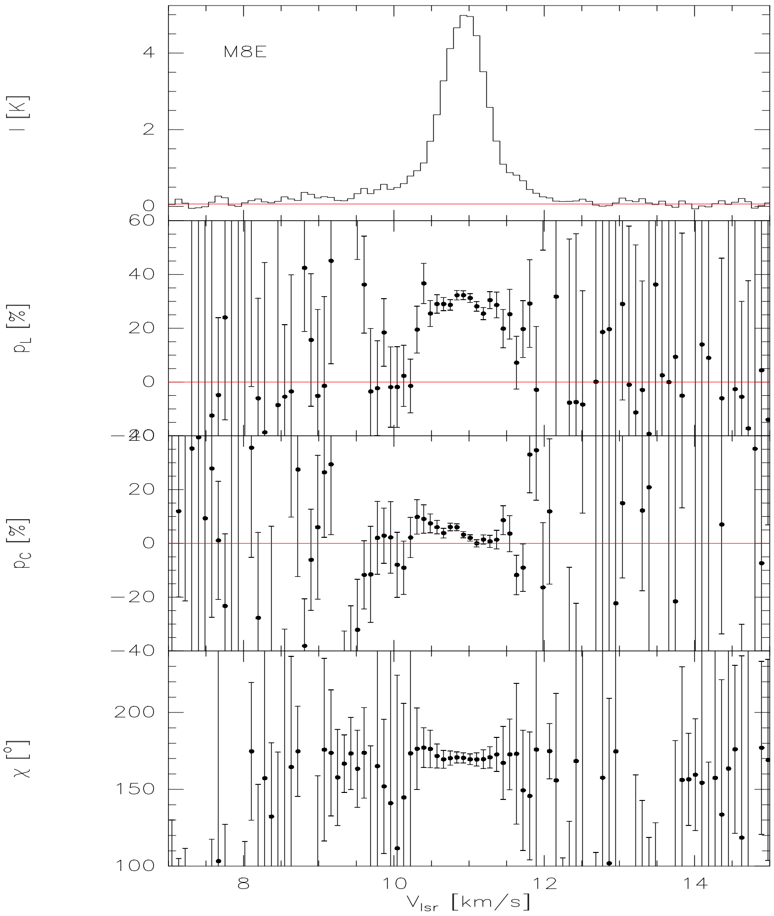


**Figure 9.**

Spectropolarimetric observation of the methanol transition $6_{-1} \rightarrow 5_0$ (E–type) at 133 GHz (Wiesemeyer et al. 2002). This class I maser source is linearly polarized in the line with a well defined position angle $\chi$. As the source has no continuum, the measurement errors increase strongly outside the line.

## APPENDIX A. POLARIMETER GAINS

The calibration factor which converts backend counts into antenna temoperature ($T_A^*$) is derived for the correlator sections $S_5$ and $S_6$ in the same way as for non–polarimetric observations. This calibration is not strictly valid for the sections $S_1$ to $S_4$ whose signal path passes through the polarimeter. Its attenuator, amplifiers, and phase shifters introduce complex *differential* gains which we describe by the $2 \times 4$ matrix $g_{ij}$. The 8 numbers give the polarimeter gain between input port $i = 1, 2$ (labelled A and B in Fig. 2) and output ports $j = 1, 4$ (labelled A+B,A-B,A*+B, and A*+B in Fig. 1) relative to the gain factor for $S_5$ and $S_6$ as described in eqs. 3-8.

$$
\begin{aligned}
S_1 &= g_{11}^2\, E_V^2 + g_{21}^2\, E_H^2 + 2\, g_{11} g_{21}\, E_V\, E_H\, cos\delta && (3)\\
S_2 &= g_{12}^2\, E_V^2 + g_{22}^2\, E_H^2 - 2\, g_{12} g_{22}\, E_V\, E_H\, cos\delta && (4)\\
S_3 &= g_{13}^2\, E_V^2 + g_{23}^2\, E_H^2 + 2\, g_{13} g_{23}\, E_V\, E_H\, sin\delta && (5)\\
S_4 &= g_{14}^2\, E_V^2 + g_{24}^2\, E_H^2 - 2\, g_{14} g_{24}\, E_V\, E_H\, sin\delta && (6)\\
S_5 &= E_V^2 && (7)\\
S_6 &= E_H^2 && (8)\\
& && (9)
\end{aligned}
$$

The relative gains $g_{ij}$ were determined by recording the response of the polarimeter output channels to a strong linearly polarized 86 GHz source (sect. 4.3). The simple relations (Tab. 2) between the Stokes parameters and the signals $S_1$ to $S_4$ as obtained in an astronomical observation are then corrected as follows:

$$
\begin{aligned}
I &= S_5 + S_6 && (10)\\
Q &= S_6 - S_5 && (11)\\
U &= \frac{1}{g_{11}\, g_{21} + g_{12}\, g_{22}} \{ \; (S_1 - S_2) \\
&\quad - \left[ \frac{g_{11}^2 - g_{12}^2}{2} + \frac{g_{21}^2 - g_{22}^2}{2} \right] I/2 && (12)\\
&\quad - \left[ \frac{g_{21}^2 - g_{22}^2}{2} - \frac{g_{11}^2 - g_{12}^2}{2} \right] Q/2 \} \\
V &= \frac{1}{g_{13}\, g_{23} + g_{14}\, g_{24}} \{ \; (S_3 - S_4) \\
&\quad - \left[ \frac{g_{13}^2 - g_{14}^2}{2} + \frac{g_{23}^2 - g_{24}^2}{2} \right] I/2 && (13)\\
&\quad - \left[ \frac{g_{23}^2 - g_{24}^2}{2} - \frac{g_{13}^2 - g_{14}^2}{2} \right] Q/2 \}
\end{aligned}
$$


## ACKNOWLEDGMENTS

We are grateful to F. Mattiocco, IRAM receiver laboratory, for measuring the broadband characteristics of the IF polarimeter on a network analyzer. The team of telescope operators headed by M. Ruiz supported commissioning activities with great patience. A. Sievers and G. Paubert, IRAM–Granada, helped at various stages. The idea of using an IF polarimeter for millimeter wavelength spectroscopy was born in conversations with W. Zinz (Max-Planck-Institut für Radioastronomie, Bonn/Germany).


## REFERENCES


1. J. D. Kraus, *Radio Astronomy*, McCraw–Hill Book Company, New York, 1966.
2. K. Rohlfs, *Tools of Radio Astronomy*, Springer Verlag, Berlin, 1986.
3. D.P.Clemens, B.D.Kane, R.W.Leach, and R. Barvainis, "Millipol, a millimeter/submillimeter wavelength polarimeter - instrument, operation, and calibration," *Publ. Astr. Soc. Pac.*, **102**, p. 1064, 1990.
4. R.Barvainis, "A multitransitional study of linear polarization in sio maser emission," *Ap. J.* , **288**, p. 694, 1985.
5. R. Crutcher, T. Troland, B. Lazareff, and I. Kazès, "CN Zeeman observations of molecular cloud cores," *Ap. J.* , **462**, pp. L79 – 82, 1996.
6. C. Heiles, P. Perillat, M. Nolan, D. Lorimer, R. Bhat, T. Ghosh, E. Howell, M. Lewis, K. O'Neil, C. Salter, and S. Stanimirovic, "All-Stokes Parameterization of the Main Beam and First Sidelobe for the Arecibo Radio Telescope," *Publ. Astr. Soc. Pac.*, **113**, pp. 1247–1273, Oct. 2001.
7. Wright and Foster, "Polarization of the crab nebula," *Astrophys. J.* **239**, p. 873, 1980.
8. T. Hagfors, "Remote probing of the moon by infrared and microwave emission and by radar," *Radio Science* **5**, pp. 189 – 227, 1970.
9. C. Thum, D. Morris, S. Navarro, and H. Wiesemeyer, "A 3mm polarization survey of active galactic nuclei," *Astr. Ap.*, , in preparation.
10. F. Herpin, A. Baudry, and C. Thum, "3mm polarization survey of SiO stars," *Astr. Ap.*, , in preparation.
11. H. Wiesemeyer, C. Thum, and M. Walmsley, "A millimeter survey of methanol polarization," *Astr. Ap.*, , in preparation.
12. R. Barvainis and C. Predmore, "Time variability of the 87 GHz linear polarization and flux density of active extragalactic objects," *Ap. J.* , **282**, p. 402, 1984.
13. L. Greenhill, C. Gwinn, C.Schwatz, J.M.Moran, and P. Diamond, "Coexisting conical bipolar and equatorial outflows from high–mass protostar," *Nature* **396**, pp. 650 – 653, 1998.